Ocean Engineering 235 (2021) 109377

Contents lists available at ScienceDirect

Ocean Engineering

journal homepage: www.elsevier.com/locate/oceaneng

Drag and inertia coefficients of live and surrogate shellfish dropper lines under steady and oscillatory flow

Jannis Landmann [a,*], Lukas Fröhling [a], Rebekka Gieschen [b], Bela H. Buck [c,d], Kevin Heasman [e], Nicholas Scott [e], Malcolm Smeaton [e], Nils Goseberg [b,f], Arndt Hildebrandt [a]

[a] Leibniz Universität Hannover, Ludwig-Franzius-Institute for Hydraulic, Estuarine and Coastal Engineering, Nienburger Straße 5, 30167 Hannover, Germany
[b] Leichtweiß-Institute for Hydraulic Engineering and Water Resources, Division Hydromechanics, Coastal and Ocean Engineering, Technische Universität Braunschweig, Beethovenstr. 51a, 38106, Braunschweig, Germany
[c] Alfred Wegener Institut, Helmholtz-Zentrum für Polar- und Meeresforschung, Bussestr. 27, 27570, Bremerhaven, Germany
[d] Applied Marine Biology and Aquaculture, University of Applied Sciences Bremerhaven, An der Karlstadt 8, 27568, Bremerhaven, Germany
[e] Cawthron Institute, 98 Halifax Street East, Nelson, 7010, New Zealand
[f] Coastal Research Center, Joint Research Facility of Leibniz Universität Hannover and Technische Universität Braunschweig, Hannover, Germany

ARTICLE INFO

Keywords:
Aquaculture engineering
Bivalves
Hydrodynamic coefficients
Drag
Inertia
Mussels
Offshore

ABSTRACT

Against the background of a drastically increased demand of marine proteins, off-bottom, bivalve aquaculture, provides significant potential for production growth when moved into more energetic marine waters. Hence, research, industry and politics are currently proposing the development of new offshore sites. The highly energetic conditions at these sites present a challenging environment for bivalve aquaculture. In this work, physical experiments of suspended bivalves provide new knowledge on the commonly used design parameters: the drag and inertia coefficients. Live bivalves and manufactured surrogate models at a 1:1 scale were tested in a towing tank as well as under waves. The drag coefficient of live blue mussels was determined to be $C_d = 1.6$ for Reynolds numbers between 2.3×10^4 and 1.4×10^5. The inertia coefficient obtained from the wave tests was $C_m = 2.1$ for Keulegan Carpenter numbers $KC < 10$. In a pursuit to better understand the differences between live mussels and surrogates in laboratory conditions, the analysis revealed that appropriate surrogates can be identified. A method to determine the characteristic diameter of mussel dropper lines is suggested. The results facilitate the future design of aquaculture systems in high-energy environments and allow for an integration into numerical models.

1. Introduction

With an increasing population, the global need for new protein sources is at an all-time high. For large populations worldwide it is important that these sources can be produced locally (Henchion et al., 2017). Cultivated marine bivalves, including oysters, mussels, and scallops (to name a few) can play an important role in this regard because all of these species may be farmed at an economically viable scale. Promotion of fish and seafood as healthy and nutritious food sources has resulted in increased demand for marine protein in developed countries (Hosomi et al., 2012). As a whole, the aquaculture industry is a fast growing food production sector with globally increasing growth rates of 5.8% between the years 2000 and 2016 (FAO, 2020). In 2018 Coastal aquaculture yielded 30.7 million tons of food fish production with a share of 17.3 million tons of shelled mollusc, constituting 56% of the combined production of marine and coastal aquaculture (FAO, 2020). In addition, replacement scenarios of red meat with aquaculture proteins have the potential to reduce terrestrial land use, and this in turn allows to cut greenhouse gas emissions through afforestation (Röös et al., 2017). As the majority of wild fisheries' stocks are being fully exploited, some unsustainably, aquaculture as an industry is presently growing to meet the increasing demand for seafood (FAO, 2020). To this end, policy makers, industry officials and researchers are advocating a move to offshore locations despite the higher energetic exposure to waves and currents. Globally, over 1,500,000 km^2 could potentially be developed for marine bivalve aquaculture according to Gentry et al. (2017) based on the relative productivity potential of ocean areas for marine aquaculture and site-selection criteria (e.g. temperature tolerance, location-specific growth potential and constraints such as allowable depth or other relevant environmental conditions). To date, longline farming systems are considered the most promising technology

* Corresponding author.
E-mail address: landmann@lufi.uni-hannover.de (J. Landmann).

https://doi.org/10.1016/j.oceaneng.2021.109377
Received 8 December 2020; Received in revised form 11 June 2021; Accepted 19 June 2021
Available online 26 June 2021

Notation

Symbol	Appellation	Dimension
C_D	Drag coefficient	[-]
C_M	Inertia coefficient	[-]
D_0	Smooth cylinder diameter	[m]
D_{char}	Characteristic diameter	[m]
D_i	Individual diameter measurement	[m]
F_D	Drag Force	[N]
F_M	Inertia Force	[N]
H_i	Wave height	[m]
L_m	Mean mussel length	[m]
L_{wet}	Wetted length of dropper line	[m]
R_p	Polygon radius	[m]
R_s	Spheroid polar radius	[m]
T_i	Wave period	[s]
$\dot{u}$	Horizontal water particle acceleration	[m/s^2]
u_a	Maximum horizontal water particle velocity	[m/s]
λ_i	Wave steepness	[-]
KC	Keulegan-Carpenter number	[-]
Re	Reynolds number	[-]
V	Volume	[m^3]
k	Roughness height	[m]
u	Horizontal water particle velocity	[m/s]
ν	kinematic viscosity	[m^2/s]
σ_i	Standard deviation	[-]

option for expanding into offshore environments as they have been shown to be the most resilient in high-energy conditions (Buck and Langan, 2017; Cheney et al., 2010; Buck, 2007). These systems commonly consist of multiple rows of dropper lines hanging from a main horizontal line, commonly called the backbone. Floats connected to the backbone provide buoyancy and station keeping is ensured via mooring lines. The dropper lines consist of a polyester or polypropylene rope at the core to which the mussels attach via their byssus threads, the bundled filaments secreted by bivalves (a - c). Fig. 1d shows a longline system with dropper lines, its key system elements as well as the motions and forces acting on it when exposed to surface gravity and internal waves as well as tidal currents.

The interactions between waves, currents and structures (cp. Fig. 1e), e g. Cylinders, are a commonly investigated research topic where the Morison equation is used to determine the hydrodynamic loads on slender structures (Morison et al., 1950). Recently, Negro et al. (2014) have noted the Morison's equation may not be valid for cylindrical offshore wind energy foundations where waves are significantly disturbed and diffracted (e.g. diameter of structure D $>$ 0.2 L, with L being wave length) when interacting with these structures. For those cases where wave diffraction can be neglected, different flow regimes around cylinders immersed into oceanic waters and the corresponding fluctuations of drag and inertia coefficients have been thoroughly investigated (Achenbach, 1971; Sarpkaya et al., 1984; Sarpkaya, 1976, 1990; Nath, 1987; Bonakdar et al., 2015). These studies focus on the influence of the roughness of cylinders, which influences the boundary layer and vortex separation near the cylinder's circumference. The difficulties to determine the hydrodynamic forces acting on irregular bodies has also been investigated by Bagheri and Bonadonna (2016), who introduced a general model for the prediction of drag coefficient of non-spherical solid particles of regular and irregular shapes. Similarly, Loth (2008) investigated the drag of non-spherical objects and discussed the aspect ratios, surface area ratios as well as the flow separation and turbulent boundary layer conditions. It has been shown that the Morison equation is applicable for ultra-rough cylinders (Wolfram and Naghipour, 1999), to which mussel dropper lines (cp. Fig. 1a–c) can be compared when they grow in suspended cultures. Plew (2005) used the assumption of ultra-rough cylinders as a model to assume a representative dropper line for theoretical research regarding the hydrodynamic implications of offshore mussel farms under current-only conditions.

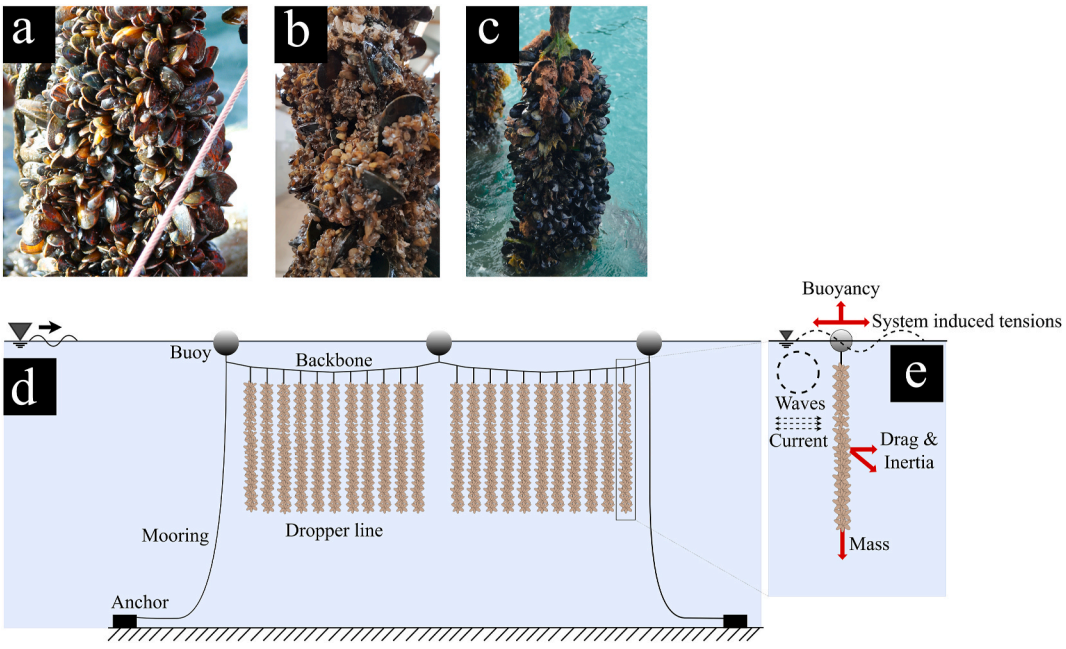

Fig. 1. Photographs of freshly harvested blue mussels (a), spat-encrusted blue mussels (b) and green-lipped mussels (c) and a schematic drawing of a longline system (d) with a detail view of a dropper line (e) and the parameters influencing it (not to scale). (For interpretation of the references to color in this figure legend, the reader is referred to the Web version of this article.)

This author concluded that the use of drag coefficients obtained in laboratory tow tests at constant velocities is not appropriate for wave force calculations. Stevens et al. (2008) provided a detailed description of the physics of shellfish aquaculture systems regarding the effect of the flow on the farm and the movement of the farm's components. In the absence of experimentally derived values, these authors proposed the use of hydrodynamic coefficients similar to rough cylinders. They concluded that further research within this highly interdisciplinary topic needs to be conducted in a multi-scale approach, e.g. as feeding and spat retention take place in an individual scale while load dynamics need to be conducted for parts of the system or the system as a whole. Towing tests have been carried out with a focus on the determination of the effect of in- and exhalent mussel jets, where a drag coefficient was determined for an artificially, re-constructed mussel dropper (Plew et al., 2009). A work by Shi et al. (2011) concentrated on a three-dimensional model modified by including two types of drag to study the dynamic coupling between physical and biological processes of an area used for suspended aquaculture. The authors showed the vertical structure of currents in a suspended aquaculture site and determined the structure caused a 40% reduction in average flow speed. Hildebrandt et al. (2018) showed, in physical model tests, that the tested mussel specimens can be assumed to have ultra-rough surfaces. A recent work by Xu et al. (2020) describes a computational fluid dynamics approach to obtaining the drag of mussel dropper lines under a tidal current. Observational studies in aquaculture farms with a focus on the hydrodynamics, stresses, motion of whole farms of mussel longlines as well as growth behaviour and stock density of the bivalves in exposed environments are also available (Gagnon and Bergeron, 2011; Díaz et al., 2011; Garen et al., 2004; Drapeau et al., 2006; Plew et al., 2005). Gagnon and Bergeron (2017) showed that the tension in, and acceleration of, submerged mussel longline farms is significantly smaller compared to surface systems. Stevens et al. (2007) identified tidal loading as a main contributor to the overall force acting on a surface longline farm and assumed that oscillating wave forces contribute significantly.

A number of aquaculture systems were investigated with respect to their loading conditions in marine currents (Gagnon and Bergeron, 2017; Zhu et al., 2020; Konstantinou and Kombiadou, 2020; Liu and Huguenard, 2020; Xu and Dong, 2018), and oceanic waves (Hildebrandt et al., 2018; Heasman et al., 2021; Landmann et al., 2019; Lin et al., 2016; O'Donncha et al., 2013; Reid et al., 2020; Zhao et al., 2019). However, research regarding the inertia coefficients C_M of mussel dropper lines is particularly scarce. Thus, contrary to the mainly observational and numerical approaches presented above, this study focuses on the hydrodynamic loads on mussel dropper lines under laboratory conditions in order to gain a better understanding of the processes around mussel dropper lines. A closer look at the available literature reveals that the following aspects of marine loading on shellfish-grown rope are not sufficiently understood or substantially covered in the scientific literature:

- Commonly, force coefficients of mussel droppers are inferred from limited towing tests (Plew et al., 2009; Hildebrandt et al., 2018), or in few cases, by using observational data from farms (Gagnon and Bergeron, 2017), yet then no control over the wave conditions exists. In other cases laboratory data is obtained through small- or mid-scale experiments (Landmann et al., 2021; Lin et al., 2016), however, there is no clear guidance as to how the complex surface of mussel droppers should be modelled.
- Comparisons between mussel droppers with live animals and their simplified surrogates used in experimental or modelling studies (Landmann et al., 2019) have not been conducted in realistic hydrodynamic conditions. It remains unclear to date, how appropriate surrogate droppers are with respect to the forces exerted on them.
- Determination of the inertia coefficient of mussel dropper lines or their surrogates through physical or numerical experiments has not been conducted for oscillatory flow regimes. As summarized by Gagnon (2019) are the hydrodynamic coefficients of mussel suspensions in waves unknown. This is the most important gap of knowledge for the further development of open ocean aquaculture because the additional peak loads generated by waves can be more than an order of magnitude larger than the current-induced forces (Landmann et al., 2021).

Based on the above-identified shortcomings in understanding of the complex flow problem evolving where currents and waves interact with shellfish-grown rope, a comprehensive experimental program has been devised. Live blue mussels (*Mytilus edulis*) as well as potentially scalable, substitute surrogate models are tested. The surrogate models, were created based on 3D-scans and the Abbott-Firestone-Curve as a surface descriptor is tested and analysed. Carriage-based steady flow experiments along the length of a flume with different velocities as well as oscillating wave tests were conducted to determine the forces acting on the dropper lines and identify drag and inertia coefficients. The specific objectives of these tests were to:

- separate the complex interdependent loads a mussel dropper is subjected to an open ocean environments and gain insight into the hydrodynamics based on comprehensive tests under laboratory conditions
- to evaluate and assess drag C_D and inertia C_M coefficients of live and surrogate dropper lines under steady as well as oscillatory flow conditions, including surface gravity waves.
- to report –for the first time-inertia coefficients for a range of live and surrogate dropper lines, in order to facilitate offshore design of aquaculture technology
- to discuss the appropriateness of the influential parameters, i.e. the characteristic diameter and shape of the dropper lines, the suitability of the created surrogates as well as the parameter ranges tested, i.e. KC number and Re numbers and the implications for further research.

2. Material and methods

2.1. Experimental setup

In order to better understand the complex loading of mussel dropper lines exposed to oceanic conditions, a comprehensive set of experiments with live-mussel dropper lines as well as surrogate bodies was carried out at the wave and towing tank "Schneiderberg" (WKS) of the Ludwig-Franzius-Institute for Hydraulic, Estuarine and Coastal Engineering of the Leibniz Universität Hannover, Germany. The WKS is 110 m long, 2.2 m wide and 2.0 m deep; its walls and bottom are made of cement plaster and smooth floating screed, respectively. The electronically-driven machine shaft (46 kW) with a maximum stroke of ±0.9 m can generate maximum regular wave heights of 0.5 m for wave periods of 2–7 s. The maximum speed of the wave board is 1.62 m/s and the maximal acceleration is 2.88 m/s^2. The opposite end has a wave absorbing beach wedge made of coarse gravel, at a slope of 1:10. The water depth was set to a constant 0.93 m during testing. The test location within the wave flume was positioned at a distance of about 60.0–65.0 m from the wave maker, where an observational window is located. A top and side view of the WKS is presented in Fig. 2.

For the tests, three 1.0–1.5 m long dropper line specimens (blue mussels originate from a farm in the Kiel fjord at the Baltic coast) as well as three different mussel surrogates with a length of 1.00 m were selected. The collector rope with live mussels (see Fig. 3, LM) were used to derive surrogate specimen, and the derivation process included sophisticated laser scanning, data modelling and curation, as well as laser-supported 3D-printing fabrication. The geometric and material features of the live- and surrogate-mussel dropper lines used in this work are depicted in a side-by-side arrangement in Fig. 3. A more detailed

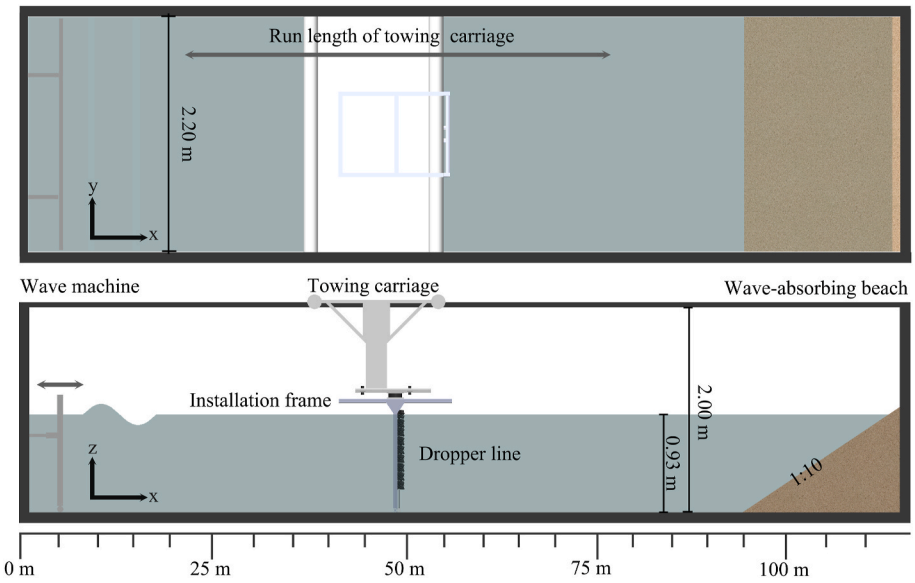

Fig. 2. Sketch of the wave and towing tank in top and side view, highlighting the run length of the towing carriage as well as the position of the wave machine and dissipative beach.

Fig. 3. Live mussel dropper line (LM) next to surrogate mussel dropper line 1 (SM 1), surrogate mussel dropper line 2 (SM 2) and surrogate mussel dropper lines 3 (SM 3).

description of procurement of the live mussels, the scanned mussel dropper lines in general as well as the surrogate models, including their creation, is available (Landmann et al., 2019). The surrogates were created based on the aforementioned 3D scanning, and the derivation process used the Abbott-Firestone approach (Abbott and Firestone, 1933) for live to surrogate model conversion, as well as statistical mean value analysis. Three types of surrogates were proposed for the geometrically similar modelling. The first surrogate is based on the average shell of the originally tested live-mussels (see Fig. 3, SM1). To that end, the length, volume, weight and width of a representative number of sample blue mussel shells were taken, and a digital average representation of blue mussel shells was developed with computer-aided design. The average model of the blue mussel shells was then arranged around a core cylinder (depicting a rope in size/diameter), by varying each shell's rotation randomly. The mean weight per unit length was chosen as a metric, and to match the surrogates overall geometry with varying angles as compared to the live blue mussels. The second surrogate as shown in Fig. 3 (SM2) is based off a laser-scanning 3D point cloud of a section of the scanned live mussels, which represents the closest fit to the weighted arithmetic average material distribution. The triangulated section estimated the facets not covered by the 3D-scan due to a blocked field of view. The third surrogate (see Fig. 3, SM3), based on the characteristic Abbott-Firestone-Curve, uses a reproduction of the weighted arithmetic average material distribution as well, but condenses the average material distribution into a simplified geometry. This was achieved by choosing a slender cylinder with 10 leave-shaped outcrops, and is proposed here as a more simple, potentially easier to build and scale surrogate, providing a novel geometric approach to future testing. The three different surrogates have been proposed in order to better understand their feedback of the different surface features with respect to uniform and oscillatory flows, and their effect on drag and inertia coefficients.

For the towing as well as the wave tests, the mussel and surrogate dropper lines were attached to a towing carriage shown in Fig. 2. The test setup, consisting of an installation frame and various measurement equipment, was rigidly attached to the carriage. Any potential deflections upon current or wave loading onto the long cantilever arm were avoided by using non-distensible wire running from the bottom of the installation frame to the top of the carriage. The vertically oriented installation frame (height x width: 1.00 m × 0.80 m) was designed for the rigid fastening of the dropper lines through clamps with an

interlocking grid at the top and bottom. The surrogates were attached to the wire using a grub screw, preventing translational as well as rotational movement.

2.2. Instrumentation

Resulting forces were recorded for the whole holding frame using a six-axis force-transducer (K6D110 ME-Meßsysteme GmbH, Henningsdorf, Germany) attached to the towing carriage. The velocity of the towing carriage was recorded during each run using an incremental rotary encoder (DBV50E-22EKA0020, SICK Vertriebs-GmbH, Düsseldorf, Germany) with a resolution of 12.5 pulses/mm and an accuracy of 4 mm/m. The time-history of the water surface elevation was recorded using two ultra-sonic sensors with the corresponding controller ULS 40-D (USS, 20130, General Acoustics, Kiel, Germany). The accuracy of the sensors is given with 0.36 mm. The sensors were recorded using an industry-grade data acquisition system, set to a sampling rate of 100 Hz. In addition, cameras were used to record each test visually at frame rate of 30 frames/s. Fig. 4 shows a photograph of the complete instrumentational set-up. A more detailed description of the setup used in this work is presented in Landmann et al. (2019).

2.3. Experimental procedures and test program

Two groups of tests were conducted to obtain drag and inertia coefficients for the different samples that were the focus of this work: (1) towing and (2) wave tests. The individual recordings of each towing test started while the carriage with installation frame and dropper line was at rest to provide a zero-load reference for each run. In addition, the installation frame was also towed along the flume axis without specimen installed in order to obtain forces of the installation frame only. These forces were later subtracted from the measurements of the tested dropper lines. Towing tests were conducted at velocities of $u_1 = 0.25$ m/s, $u_2 = 0.50$ m/s, $u_3 = 0.75$ m/s and $u_4 = 1.00$ m/s. The towing velocities were recorded during each run by transforming the rotational speed data obtained from the incremental rotary encoder into an equivalent forward speed. Each dropper line was submerged over a wetted length of $L_{wet} = 0.80$ m, measured while the installation frame was at rest. The fastening clamps at both ends, which were securely tightened, created the vertical tension inside the dropper lines. This ensured an equal flow velocity along the whole length of the dropper line during the towing tests. Each test was conducted up to three times for testing repeatability, and overall 72 towing tests were conducted.

Secondly, the wave tests were conducted in front of the observational window, installed in one sidewall of the flume, where the towing carriage was rigidly fastened. The wave heights tested were $H_1 = 0.10$ m, $H_2 = 0.12$ m and $H_3 = 0.15$ m with wave periods of $T_1 = 1.20$ s, $T_2 = 1.65$ s and $T_3 = 2.40$ s. Each test was conducted up to three times for testing repeatability, and 72 wave tests were conducted in total. Again, in order to obtain the forces acting only on the dropper lines, the installation frame was tested without the dropper lines in zero tests, for later subtraction of these forces. The overall test parameters in aggregate form are listed in Table 1.

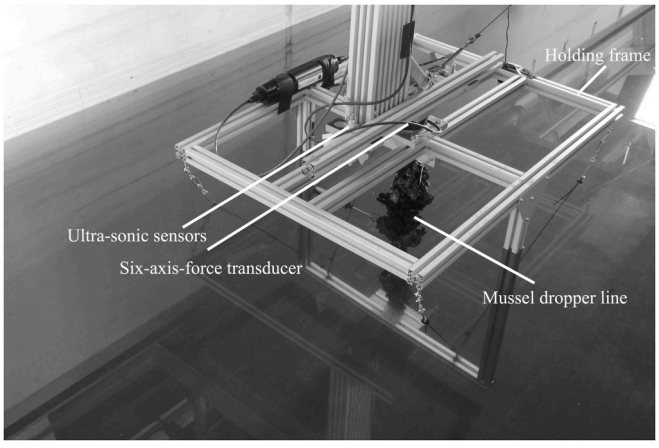

Fig. 4. Installation frame with measuring equipment and a sample, live mussel dropper line attached.

3. Theoretical background and data processing

For the analysis of the responses of offshore structures to oceanic waves, the forces acting on slender bodies are most commonly estimated using the Morison approach (Morison et al., 1950). This allows the calculation of forces on slender bodies fixed in waves or bodies oscillating in still water or waves (DNV, 2010a). The Morison equation provides an efficient approach for the calculation of arbitrary complex structures while the C_D- and C_M-coefficients take into account vortex shedding effects, non-static effects as well as the surface roughness of the structure. Thus, complex flow problems can be solved. Assuming that the dropper lines that were tested could be –at first order-approximated as a rigid, slender cylinder, the quantification of the drag and inertia coefficient for the different dropper lines through dedicated force and velocity measurements is possible. This assumption is based on the accepted use of hydrodynamic coefficients in aquaculture research (Wolfram and Naghipour, 1999; Plew, 2005; Stevens et al., 2008; Plew et al., 2009; Gagnon, 2019) and industry projects. The determination can be based on the Morison equation:

$$F = \frac{1}{2}\rho C_D u^2 A + \rho C_M V \dot{u} \qquad \text{Eq. (1)}$$

where F is the total horizontal force, $\rho = 1000\frac{kg}{m^3}$ is the density of the fresh water in the flume, C_D is the drag coefficient, u is the horizontal particle velocity, $A = L_{wet}{}^*D_{char}$ is the referential front face area composed of the wetted length of tested structure L_{wet} and the characteristic diameter D_{char}, C_M is the inertia coefficient, V is the volume of the structure and $\dot{u}$ is the flow particle acceleration. The wetted length $L_{wet} = 0.80\,m$ was kept constant for all tested dropper lines. The first term of equation (1) corresponds to the drag forces acting on the dropper line, while the second term describes the inertia forces contributed by the flow acceleration through wave motion. For the drag tests in steady-state flow conditions, the equation simplifies to the first term only, as no acceleration occurs; it then reads:

$$F_D = \frac{1}{2}\rho C_D u^2 A \qquad \text{Eq. (2)}$$

where F_D is depicting the drag force acting on the dropper lines. More

Table 1
Test parameter for drag- and wave-tests with velocity, wave height, wave period and wave steepness. Re- and KC-numbers, where, u is the velocity of the current or the towing carriage, D_{char} is a characteristic diameter of the observed body, ν depicts the kinematic viscosity of the fluid, u_a is the maximum horizontal component of the orbital velocity of a wave at the water's surface and T is the wave period, are given for the live mussels.

Steady flow experiments				
Velocity [m/s]	$u_1 = 0.25$	$u_2 = 0.50$	$u_3 = 0.75$	$u_4 = 1.00$
$Re - number = \frac{u^*D_{char}}{\nu}\,[-]$	3.0×10^4	5.6×10^4	8.0×10^4	1.0×10^5
Wave tests				
	Wave 1	Wave 2	Wave 3	
Wave height [m]	$H_1 = 0.10$ m	$H_2 = 0.12$ m	$H_3 = 0.15$ m	
Wave period [s]	$T_1 = 1.20$ s	$T_2 = 1.65$ s	$T_3 = 2.40$ s	
Wave steepness [-]	$\lambda_1 = 0.04$	$\lambda_2 = 0.03$	$\lambda_3 = 0.02$	
$KC - number = \frac{u_a{}^*T}{D_{char}}[-]$	$KC_1 = 1.5$	$KC_2 = 4.0$	$KC_3 = 7.5$	

specifically, in this work, the drag coefficient C_D can be also written as:

$$C_D = \frac{2^* F_D}{\rho u^2 A} \quad \text{Eq. (3)}$$

The drag coefficient is related to the Reynolds number (Reynolds, 1883) *Re*, expressed by:

$$Re = \frac{u^* D_{char}}{\nu} \quad \text{Eq. (4)}$$

where u is the velocity of the current or the towing carriage, D_{char} is a characteristic diameter of the observed body and ν depicts the kinematic viscosity of the fluid. The characteristic diameter chosen using the Morison equation, the flow parameters and the observed structure's geometry are essential. The flow parameters are the horizontal velocity u and horizontal acceleration $\dot{u}$, which are determined according to Stokes 2nd order wave theory. An exact determination of the structural parameters is however not straightforward. Mussel dropper lines are highly, irregular 3D objects, of which the referential area A and the referential volume V are hard to quantify. Cavities, crevasses and protrusion of individual mussel species into the water column make the frontal area, which is blocked for the flow, a matter of discussion. For the utilization of the Morison equation, the irregular shape of the dropper lines is approximated by a cylinder with a wetted length L_{wet} and the characteristic diameter D_{char}. The quantity L_{wet} is determined as the submerged depth, beneath the still water line plus the water surface elevation. The characteristic diameter D_{char} diverges over the length of the dropper and, as said, is challenging to estimate. For the results presented in this study, a 3D-scan of the live mussel dropper lines and a subsequent determination of the width at regular intervals along the length yielded an average characteristic diameter. The average diameters of the surrogates were determined based on the 3D-models (Landmann et al., 2019). If the number of individual measurements D_i is large enough, the projected area can be determined and, divided by number of measurements n. This provides a close approximation of the characteristic diameter, that is $D_{char} = \frac{1}{n}(\sum_{i=1}^{n} D_i)$. The determined characteristic diameter of the live mussels is $D_{char,\ LM} = 10.3$ cm and for the surrogates $D_{char,SM1} = 10.3$ cm , $D_{char,SM2} = 12.1$ cm and. $D_{char,SM3} = 13.6$ cm.

Under realistic offshore conditions, currents could deflect the dropper lines with respect to the earth' vector of gravity depending on the mass of the mussels and the velocity of the current. To account for these effects the Morison equation can been adapted to include the yaw angle of the dropper lines. However, the yawing of the dropper lines is a load evasion mechanism. In their original position, hanging vertically suspended from the backbone, the dropper lines have the largest referential area. With the introduction of a current, the dropper lines are yawed, reducing the referential area and the possible force acting on the aquaculture system. In this study, the authors' opted for an engineering approach focusing on save hydrodynamic coefficients, i.e. higher forces on the dropper lines.

3.1. Steady flow experiments

For the pre-processing of the steady-state, towing experiment group, the data sets were first cleaned of frequency components associated with carriage motions and signal noise via a Fast-Fourier-transformation. Next, a fourth-order low pass Butterworth-filter with a cut-off frequency of 3 Hz was applied to the data of the force transducer. For the analysis, a starting point was set for each towing run, when the velocity of the towing carriage has finished the acceleration phase, i.e. the turning point at the transition from increasing to constant velocity is determined. An end point was set to be when the velocity starts to decrease again from the set velocity. The forces of the installation frame, herein called zero tests, were subtracted from the measurements with the dropper lines, to isolate the force contribution of the dropper lines. To that end, Equation (2) was solved for the zero tests and the C_D-coefficients for varying Reynolds numbers were obtained. A linear function was fitted through the data points, which shows that the drag coefficient of the holding frame is within a range of $C_D = 1.72$ to 1.77 for Reynolds numbers of 1.0×10^4 to 1.3×10^5. The function of the C_D-coefficients was used to solve Equation for all unknown values of the reduction force based on the measured velocity of the towing tests with the dropper lines. This way, the quadratic influence of the velocity on the force is accounted for and the influence of the holding frame on the forces acting on the mussel dropper lines was removed. By this procedure the C_D-coefficients of the dropper lines were determined by excluding the effects of the surrounding test equipment. The unfiltered and filtered time series of the force in x-direction and the towing velocity for a test run with an approximated speed of 1.0 m/s are shown in Fig. 5. The actual forces, i.e. the C_D-dependent force without the influence of the frame, is also shown.

3.2. Oscillatory flow experiments

Equation (1) was solved with the drag and inertia coefficients as unknowns as velocity and acceleration of the water particles fluctuate under the orbital motion of the waves. A common approach to solve for the unknown force coefficients is the least squares method (Wolfram and Naghipour, 1999; Hildebrandt et al., 2009), which was also used in this work. It compares the theoretically determined and the measured forces, and then optimizes for the errors between those by using the least square method iteratively. The theoretical force is calculated based on the water elevation determined by the appropriate wave theory, which has been determined based on an analysis of the waves shown in Table 1.

The data of the wave tests were analysed via a Fast-Fourier-transformation and a fourth-order, low pass Butterworth-filter with a cut-off frequency of 3 Hz to eliminate frequency components associated with signal noise. Starting- and endpoints of the data records were set by identifying the target wave height after ramp-up of the wave maker. Each wave between these points is identified individually via zero-downcrossing (Dean and Dalrymple, 1991) and the wave height, period and length were determined. The influence of the installation frame on the force measurements was taken into account by subtracting zero test forces (frame-only) from the forces measured when testing the actual specimen.

For the theoretical force, the appropriate wave theory was determined by comparing the measured water elevation. For all waves in the experimental program Stokes 2nd order theory, according to the Le Méhauté diagram (Le Méhauté, 1976) were found to be a good approximation. Subsequently, the horizontal velocity $u(t, d)$ and

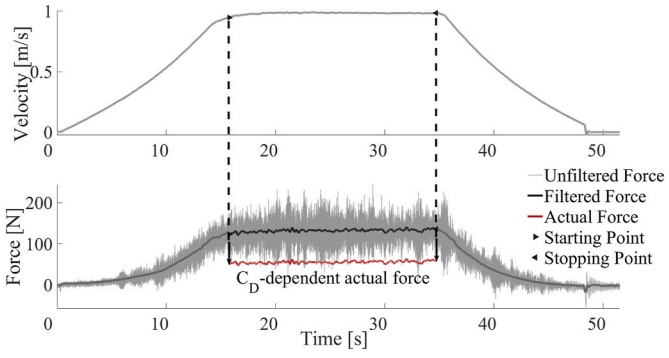

Fig. 5. Exemplarily data time series for the calculation of the drag coefficient CD with the velocity of the towing carriage, starting and stopping points for analysis and corresponding unfiltered, filtered and actual force in x-direction displayed for set velocity of 1 m/s. Vertical lines indicate starting and stopping points between which the data is used for analysis.

horizontal acceleration $\dot{u}(t,d)$ of the water particles were calculated for each time step and over the depth of the water column. The resulting parameters were used to determine the theoretical forces for the wetted length of the dropper line according to the Morison equation (Morison et al., 1950) with varying C_D and C_M between 0.01 and 6.0. Thus, the theoretical horizontal loading on the dropper lines could be estimated as a function of the drag and inertia coefficients and the smallest mathematical error between the measured and theoretical value was used as an approximation of C_D and C_M. The Keulegan-Carpenter number KC is used as a reference, as it captures the variation in the measured drag and inertia coefficients. Introduced by Keulegan and Carpenter (1934), KC is denoted as:

$$KC = \frac{u_a{}^*T}{D_{char}} \qquad \text{Eq. (5)}$$

where, u_a is the maximum horizontal component of the orbital velocity of a wave at the water's surface, T is the wave period, and D_{char} is the characteristic diameter of the observed body. Fig. 6 shows the water elevation of a measurement with a wave height of 0.10 m and a wave period of 1.2 s. The observed time series as well as all interpolated zero-crossings are highlighted. Furthermore, all resulting single waves and the corresponding forces are displayed with an indication of the theoretical wave height according to Stokes 2nd order wave theory.

4. Results and discussion

4.1. Steady flow experiments

In the experiments reported herein, Reynolds numbers ranged between $Re = 2.3 \times 10^4$ and $Re = 1.4 \times 10^5$. This covers the sub-critical flow regime under steady currents and corresponds to the current velocities expected in marine environments. The overall results regarding the steady flow experiments are shown as a scatter plot (cp. Fig. 7). The drag coefficients are plotted as a function of the corresponding Reynolds numbers. Horizontal lines indicate the overall median values for all corresponding tests, for both live mussels and the tested surrogate models. As can be seen, the median drag coefficients of the live mussel dropper lines is $C_{D,LM} = 1.6$. The drag coefficients of the three surrogates were generally lower than the live mussel results, with median values of $C_{D,SM1} = 0.9$ for the first, $C_{D,SM2} = 1.0$ for the second and $C_{D,SM3} = 0.8$ for the third surrogate type. The data points of each test are shown in grey scale and the median values of each test are depicted as colored cross symbols. The statistical median value was chosen as a descriptor as it is robust against outliers. Outliers present in the data contribute to the large spreading. As mentioned before, the force contribution of the test

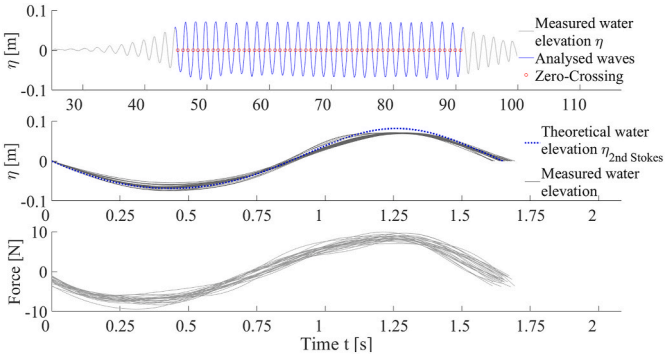

Fig. 6. Data basis for the calculation of the drag and inertia coefficient CD and CM fora wave height of 0.12 m and a wave period of 1.65 s with water elevation, analysed time window (top), theoretical and recorded waves (middle), and displayed wave x-force components of the analysed time window. Vertical lines indicate starting and stopping points between which the data is used for analysis.

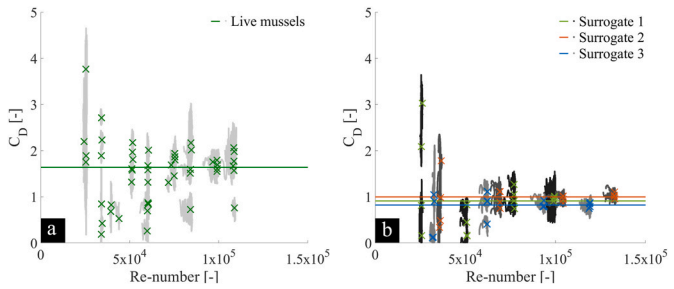

Fig. 7. Drag coefficient of mussel dropper lines (a) and surrogates 1–3 (b) with an indication of the median drag coefficients obtained from steady flow experiments as colored crosses. Exemplary, the sorted distribution of the drag coefficient of a single test is shown (a.1).

frame was separated from the force contribution of the mussel dropper lines via a C_D-dependent mathematical adjustment of the measured forces. With the subtraction of the zero-test forces, the measured load level was reduced and this, in combination with vibrations in the velocity measurements from the rotary encoder, leads to the outlying low drag values especially for lower Reynolds numbers. Fig. 8 exemplary shows the cumulative distribution function of the drag coefficient of a single test at 0.25 m/s as well as a boxplot of the same data set. It is shown, that most data points are scattered around the unifying median value, indicated again through a colored cross at $C_D \approx 1.6$. The outliers characterized by a steep increase or decrease account in the cumulative density function for less than 3% of all data points. These outliers are shown in red in the boxplot. The standard deviation of the median drag values, as a measure of the square root of the variance, is $\sigma_{LM} = 0.65$ and for the surrogates $\sigma_{SM1} = 0.71$, $\sigma_{SM2} = 0.30$ and $\sigma_{SM3} = 0.29$. The large standard deviation for SM1 is due to the scattering at low Reynolds numbers and the mentioned vibrations of the test carriage. The use of three different lengths of dropper lines during testing explains the larger variance of the live mussels, in comparison to the surrogates. These live dropper lines varied in diameter and mass and exhibited natural variations in mussel density and marine growth, i.e. soft growth like algae, anemones or sponges and secondary seeding. The inclusion of them in one dataset increases the amount of data available and the confidence in the results while slightly aggregating the variance. For Reynolds numbers larger than$Re = 6.5 \times 10^4$, a clustering of the drag coefficients is apparent as the mussel shells and the edges of the surrogate bodies promote flow separation. This behaviour has been observed in the comparison of smooth and highly rough cylinders, where rough cylinders show near constant drag coefficients while the drag coefficients of smooth cylinders change significantly with Reynolds numbers (Allen et al., 2001). This is why constant values were used as an indication of the drag coefficient. Less outliers, or conversely, closely-scattered data points, coincide with the increasing velocity. The relative error of the drag coefficients is largest where towing velocities are lowest, i.e. when

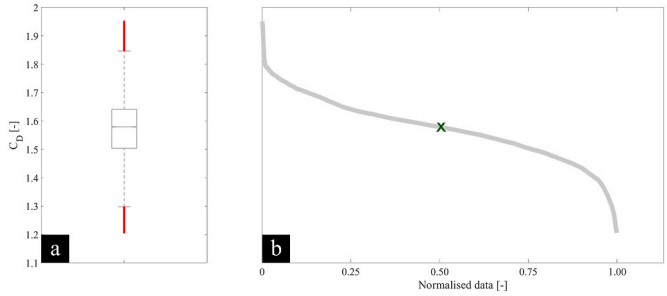

Fig. 8. Exemplary distribution of all calculated drag coefficients of a single test at 0.25 m/s displayed as a boxplot (a) and as a cumulative distribution function (b) with an indication of the median value as a colored cross.

the measured force is lowest. These current velocities around 0.1 m/s to 0.2 m/s are potentially influenced by the quality of the force measurements. Compared to realistic oceanic conditions, the range of small towing velocities is not as relevant for the design of marine aquaculture farms as the higher flow velocities; yet, for the sake of completeness are still reported here (Heasman et al., 1998). In regard to investigations pertaining to limiting biological factors, e.g. seston concentration and initial mussel growth (Rosland et al., 2011), number of mussels in a cluster including attachment properties (Brenner and Buck, 2010), as well as hitchhiker/fouling organisms on the mussel shell (Telesca et al., 2018), further investigations for even smaller Reynolds numbers might be required. This will remain an activity for future research.

4.2. Oscillatory flow experiments

An objective of these tests was to determine the hydrodynamic parameters under waves. With measured velocities and characteristic diameters based on the average diameter, Keulegan-Carpenter numbers ranged from $KC = 1.9$ to $KC = 8.8$. For small KC-numbers, results from steady-state flow experiments for the drag coefficient are not comparable to the results of the wave tests as the flow regime around marine cylinders is strongly inertia dominated (Denny, 1995). Drag coefficients become comparable when KC numbers roughly larger than 30 are considered (Sumer and Fredsoe, 2006). Therefore, the use of separate coefficients for steady and oscillatory flow is recommended (Nath, 1987; Wolfram and Naghipour, 1999; Sarpkaya, 1987).

Fig. 8 provides an overview of the calculated drag and inertia coefficients based on the live dropper lines, and the surrogate dropper lines. These are given as a function of the KC number, along with the individual data as well as median values. The approximated median drag and inertia coefficients for the live mussels are $C_{D_{LM}} = 2.3$ and $C_{M_{LM}} = 2.1$. For the surrogates the hydrodynamic coefficients are $C_{D_{SM1}} = 2.4$, $C_{D_{SM2}} = 2.8$ and $C_{D_{SM3}} = 4.4$ and $C_{M_{SM1}} = 2.3$, $C_{M_{SM2}} = 2.9$ and $C_{M_{SM3}} = 4.9$. The mathematically best solution determined by the least-square optimization is strongly dependent on the inertia coefficient and less dependent on the drag coefficient. This results in explicit solutions for the inertia coefficient, while the solutions for the drag coefficient are prone to larger scattering. The mathematically lowest error was determined as correct. A weighted least square approximation of the Morison equation might provide more explicit results regarding the drag coefficient, but is not necessary for the small KC-numbers covered in this study due to the inertia dependence. A possible source of uncertainties in the determination of the inertia coefficient is the oscillatory movement of the dropper line under the waves as well as the movement of the live mussels themselves. In the study at hand rigid fastening as well as the short length of the dropper line prevents any major deflection which permits the use of the Morison equation. However, for tests on a larger scale a deflection of the dropper like can be expected and needs to be considered. Similarly, the individual motion of live mussels will take a stronger effect on a larger scale. The similarity in the results between the rigid surrogates and the more flexible live mussels shows that the influence of movable mussels can be neglected for this setup.

4.3. Characteristics of developed surrogates

One of the objectives of this work was to better understand, how well live mussel specimen can be modelled hydro-dynamically by developing geometrically similar surrogate models. By comparing the steady-state-, and oscillatory-based drag and inertia coefficients, a better understanding of the characteristics of the surrogates can be gained. Results show that the hydrodynamic coefficients of the surrogate bodies differ from those of the live mussel dropper lines. Specifically, the results regarding the drag coefficients of the surrogates for steady-state flow experiments are 77.8%, 60.0% and 100.0% lower for surrogate 1, 2 and 3 than the results of the live mussels, respectively. For oscillatory flow experiments, the results are 4.3%, 21.7% and 91.3% higher, respectively. The inertia coefficients of the surrogates exceed the results of the live mussels by 9.5%, 38.1% and 133.3%, respectively. Given the ranges of drag and inertia coefficients, surrogate 1 (SM1) is proposed as the most similar and hydrodynamically suitable surrogate model of the live blue mussel dropper lines. The reasons for this are given below.

One reason for why such large differences were observed is due to the natural properties of the tested live mussels. Dropper lines consist of hard growth composed of multiple mussels of varying size but similar shape Live mussel are moreover very often overgrown with soft growth that is tissue of e.g. various algae species (Atalah et al., 2016). More specifically, the soft growth comprises varying species of algae, anemones, and sponges and varies strongly depending on environmental conditions such as water depth, temperature, salinity, predation as well as competition and availability of food and space (Wolfram and Theophanatos, 1985; Joschko et al., 2008). This soft growth likely has a large influence on the boundary layer development and was not recreated during the modelling of the surrogates which were made of smooth 3D-printing material. The live dropper lines, which were taken from in-situ cultures, had considerable soft growth, as can be seen in Fig. 3 (LM). Mussels, i.e. the hard growth, form the main component of the dropper lines and are strongly affected to change as the mussels mature. The surface roughness increases as the outcropping mussels grow to a harvestable size. Simultaneously, the drag coefficient increases with the surface roughness and thus drag loads on the structure become more influential. This is another reason for the differences between the live mussels and the surrogates as only a macroscopic roughness was incorporated in the models, e.g. the individual growth stages of single mussels were not considered. Surrogate 1 was based on clean, smooth average mussels. Surrogate 2 and 3 instead, were based on the weighted arithmetic average material distribution where unrepresentative peaks and valleys were filtered out resulting in a smoother surface. Therefore, with soft growth and natural variations the surface roughness of the live mussel dropper lines was higher compared to the surrogate models. The increased roughness affects various aspects of the flow around the mussel dropper lines such as hydrodynamic instabilities, i.e. vortex shedding, the interaction of vortices, the separation angle, the turbulence level as well as the vortex strength (Hildebrandt et al., 2009; Obasaju et al., 1988; Chakrabarti et al., 2016). Therefore, it can be assumed that the increased drag of the live mussels in the steady-state experiments is due to an increase in dropper diameter caused by the additional soft growth and a larger roughness. This is supported by the results of Wolfram and Theophanatos (1990) regarding the effects of marine growth on cylinders as well as more recent numerical studies by Xu et al. (2020). The lowest deviation from surrogate 2, where soft growth was incorporated by the 3D scanning further supports this assumption. Another reason for the variances are the obvious differences in shapes between live mussels and surrogates. Fig. 9 depicts the single elements of each surrogate used to construct the dropper lines. While the mussel shells, or mussel-like outcrops of surrogate 1 and 2, provide sharp edges, which promote flow separation, has surrogate 3 a rather rectangular referential area. It can be assumed that this promotes the

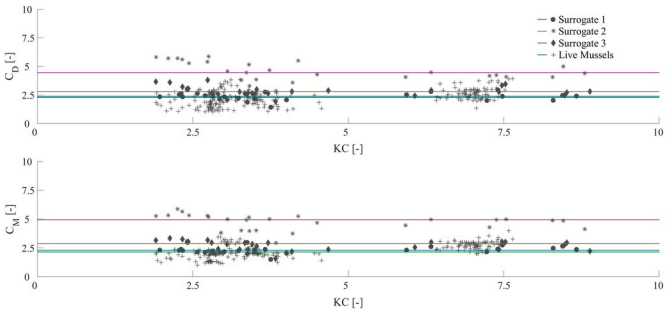

Fig. 9. Drag C_D and inertia C_M values for live mussels and surrogates over Keulegan-Carpenter number with an indication (line) of the median value.

forming of a large wake.

For the wave tests, the results regarding the drag and inertia coefficient are more consistent. The inertia dominance in the oscillating flow regime is surely a reason for a far better fit, while the above observations pertaining to drag coefficients in steady-state conditions mostly still apply. Concluding, we hypothesize that the differences regarding the hydrodynamic coefficients between the live mussels and surrogates are mostly due to natural growth on the live mussels, as well as and variations in surface roughness, flow regimes and referential frontal areas. While current-only conditions are not adequately reproduced, a satisfactory representation of the live mussel dropper lines, considering wave conditions is found. As said before, surrogate 1 (SM1) seems closest to represent the characteristics found. Surrogate 3 (SM3) is dismissed as it differed strongly under oscillatory test conditions as well as surrogate 2 (SM), which is rejected due to its complex shape, which is too specific for a generic surrogate approach.

4.4. Influence of the characteristic diameter

The characteristic diameter chosen for the determination of the drag and inertia coefficients in this study is challenging to estimate as mussel dropper lines are natural structures with uneven growth, cavities, crevasses and protrusions. To provide a better understanding of the importance of the chosen characteristic diameter alternative approaches used in literature are compared to the average diameter used in this study (see Fig. 11).

One alternative approach to express the frontal area is based on the non-dimensional surface roughness $\Delta = \frac{k}{D_0}$ of long slender cylinders (DNV, 2010b), using a spatial organization model introduced by Gagnon (2019). This approach uses the packing geometry of mussel shells around a dropper line and estimates the roughness height k as $k = \frac{0.5*L_m+R_s-R_p}{2R_p}$ with L_m being the mean mussel length, R_s the distance between the axis of the dropper line and the center of the modelled mussel and R_p the radius of the polygon on which the model is based. Following the spatial organization model allows to solve for an average mussel length of 4.7 cm and smooth cylinder diameters D_0, on the basis of the Abbot-Firestone curve provided by Landmann et al. (2019). The resulting roughness height is 2.63 cm, which results in a characteristic diameters of $D_{char,LM} = 8.6$ cm for the live mussels and $D_{char,SM1} = 7.3$ cm, $D_{char,SM2} = 8.6$ cm and $D_{char,SM3} = 8.9$ cm for the surrogates. Another approach for the determination of the frontal area in a laboratory is based on the displaced volume (Plew, 2005). The characteristic diameter can be determined as $D_{char} = \sqrt{4V/\pi L}$, with V being the displaced volume and L_w the wetted length of the dropper line. The displaced volume was determined by submerging the mussels into a cylinder filled with water with a radius of 39.0 cm and measuring the water level rise. For the live mussels with a volume of 0.013 m^3, a characteristic diameter of $D_{char,LM} = 9.2$ cm was determined. For the surrogates, characteristic diameters of $D_{char,SM1} = 7.3$ cm, $D_{char,SM2} = 7.2$ cm and $D_{char,SM3} = 7.4$ cm were determined. As all surrogates are porous, the characteristic diameters obtained are smaller in comparison to the other methods. However, these approaches are, not easily applicable for measurements in the field. Plew et al. (2009) suggested defining the characteristic diameter as $D_{char} = 2\,x\,L_{Mussel}$ with L_{Mussel} as the average mussel length. This method can easily be applied and compared to visual inspections on site. The accuracy of this estimation is however prone to errors regarding natural variations of the dropper lines and different cultivated species. For this approach, the average mussel length was determined as 4.7 cm and a characteristic diameter of 9.4 cm is assumed for live mussels and surrogates. The authors recommend the use of 3D-scans and the average diameter for experiments under laboratory conditions as the most explicit representation of the characteristic diameter can be achieved. The characteristic diameters calculated according to the above-mentioned approaches are displayed in Table 2.

Given the above-derived characteristic diameters of the live and surrogate dropper lines, a new determination of the drag and inertia coefficients can be conducted. The resulting differences in the drag and inertia coefficients are shown for the oscillating flow conditions, for the live mussels only and displayed in Fig. 10. A comparison to the suggested surrogate SM1 is possible via the indicated horizontal lines representing the results as seen above. The resulting drag and inertia coefficients are grouped for each tested set of waves to display changes induced by rising KC numbers. It can be seen that small differences in the characteristic diameter lead to comparatively large changes regarding the resulting hydrodynamic coefficients. This effect seems to increase with rising *KC*-number. A decrease of 8.7% in characteristic diameter, i.e. the difference between the average diameter and the multiple of the mussel length, results in an increase of the drag coefficient from 1.8 to 2.2 or 18%. The inertia coefficient rises from 1.95 to 2.3. This strong sensitivity of the hydrodynamic coefficients concerning the characteristic diameter can be confirmed for all results. While the change in loads due to varying diameters is not accounted for, highlights this the importance of a sensible choice regarding the characteristic diameter used for the calculation of forces in the Morison equation. The best agreement of the SM1 can be seen for the average diameter. As for rising KC-numbers, the other methods increase drastically. The authors' assume that the aforementioned influence of the soft growth and the high roughness lead to a larger characteristic diameter than suggested by the methods currently employed. Further tests with the aim of creating a referential cylinder are advised. Said cylinder would vary for the surrogate and the live mussels as the soft growth greatly influences the results. However, the referential cylinder could be used as an easy to implement body in numerical studies. The diameter of the referential cylinder will be larger than the characteristic diameter of the mussel

Table 2
Characteristic diameters of live mussels and surrogates determined according to four different approaches based on the average diameter, a spatial organization model to determine the roughness height of a mussel encrusted cylinder, the displaced volume of the dropper lines and a multiple of the mussel length.

	Live mussels	Surrogate 1	Surrogate 2	Surrogate 3
Average diameter (Landmann et al., 2019) $D_{char} = \frac{1}{n}\left(\sum_{i=1}^{n} D_i\right)$	0.103 m	0.103 m	0.121 m	0.136 m
Multiple of mussel length (Plew et al., 2009) $D_{char} = 2\,x\,L_{Mussel}$	0.094 m			
Spatial organization model (Gagnon, 2019) $D_{char} = \frac{0.5*L_m + R_s - R_p}{2R_p} + D_0$	0,086 m	0,073 m	0,086 m	0,089 m
Displaced volume method (Plew, 2005) $D_{char} = \sqrt{4V/\pi L}$	0.92 m	0.073 m	0,072 m	0,074 m

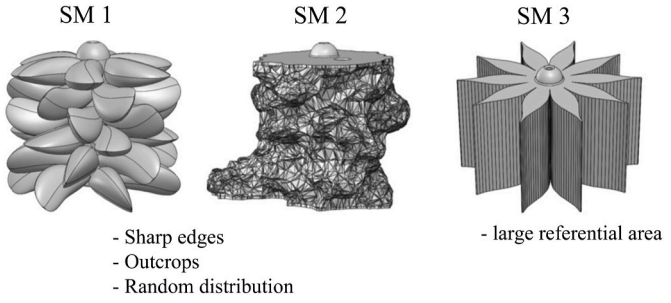

Fig. 10. Sketches of the three surrogates (LM1, LM2 & LM3) tested in this study with an indication of their most prominent features.

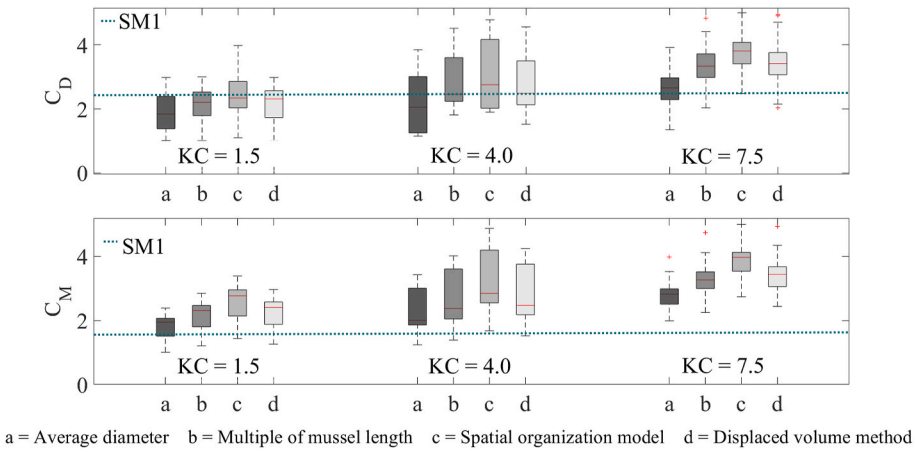

Fig. 11. Comparison of relevant characteristic diameters based on (a) the average diameter, (b) a multiple of the mussel length, (c) a spatial organization model and (d) the displaced volume for the live mussels. The compared results are grouped for each tested set of waves. The original median value from SM1 is given (line) as a comparison.

dropper lines as the increase in drag through soft and hard growth needs to be compensated. In the absence of this data, we recommend using the average diameters for the design of mussel dropper lines or longline farms.

4.5. Comparison to existing studies

The results of the live mussels that were tested experimentally are compared and discussed in the light of other published studies. This discussion only references the data regarding drag coefficients. As mentioned in a review by Gagnon (2019), inertia coefficients of mussel dropper lines have not been experimentally determined before; only now these have become available through the work reported herein. In numerical studies, the dropper lines are modelled as cylinders of varying diameter to which the Morison equation is applied and drag coefficients have been assumed as $C_D = 1.5$ (Raman-Nair and Colbourne, 2003) or $C_D = 1.2$ (Raman-Nair et al., 2008). The authors stress the necessity of physical experiments or field tests to obtain realistic values as no basis for their assumptions is given. A more recent investigation assumes $C_D = 1.1 - 1.7$ as realistic values for the modelling of submerged shellfish longlines (Knysh et al., 2020) based on a literature research. Their numerical model of a longline aquaculture system showed little sensitivity to the exact choice of drag coefficients regarding the predictions for mooring line tensions and longline dynamics. Detailing the overall physics of offshore shellfish aquaculture, Stevens et al. (2008) suggest values of $C_D = 1.5$, linked to research regarding ultra-rough cylinders. Xu et al. (2020) assumed the drag coefficient of mussel dropper lines to range from $C_D = 1.1$ to 1.2 based on a computational fluid dynamics approach through a 3D-Large Eddy Simulation. None of the assumptions mentioned above are based on validated physical experiments and should be considered as an estimate. While results regarding drag and inertia coefficients of cylinders with varying roughnesses are readily available, are results for physical experiments scarce. In a study regarding the hydrodynamic implications of offshore shellfish systems, a provisional drag coefficient was determined using towing tank tests on a length of dropper line (Plew et al., 2005). The characteristic diameter was based on the multiple of the mussel length, as described above, and resulted in a characteristic diameter of 0.16 m. A resulting drag coefficient of $C_D = 0.89$ was determined. In a later investigation a drag coefficient of $C_D = 1.27$ was determined through physical model experiments (Plew et al., 2009). A possible weakness is the used test setup, where mussel shells (*P. canalicus*) were glued onto 10 mm polythene hoses to imitate dropper lines and no comparison to live-like conditions is given. Gagnon and Bergeron (2011) report on tests conducted with four 4 m long dropper lines where a drag coefficient of $C_D = 1.25$ was determined. The dropper lines were cut by divers and dragged behind a boat where a load cell was located. The influence of waves and current was not included in the results, which affects the outcome. The results of all mentioned studies are summarized in Table 3, with Reynolds numbers specified if possible. The compiled data show that the available research regarding hydrodynamic coefficients is mainly based on theoretic considerations and numerical approaches without validation. Furthermore, the studies regarding physical experiments are of varying quality as either the dropper lines or laboratory conditions are improvable. However, precise physical experiments are necessary to accurately predict the forces acting on aquaculture systems in the open ocean during the design stage. The hydrodynamic coefficients determined in this study supplement the currently available data, give a more reliable estimation, and extend the available hydrodynamic parameters with the inclusion of physical model tests in oscillating flow regimes.

5. Conclusions

This work is related to the design and testing of new marine aquaculture concepts. During the planning and assessment of marine aquaculture projects, there is a need to determine the forces acting on the structural components for efficient designs. Mussel laden dropper lines form the bulk of the mass and surface area of a longline mussel farm. Therefore comprehensive physical model tests were conducted to determine the hydrodynamic coefficients of live mussel dropper lines under laboratory conditions in the present study. This enables planners and researchers alike to quantify the influence and impact of a single dropper line and assess their combined effect in a farm. The main conclusions of this study can be summarized as follows:

Table 3
Reported values of dragC_D and inertia$C_M$coefficients for mussel dropper lines. Ranges of tested Reynolds numbers and Keulegan-Carpenter numbers are indicated.

Source	Steady flow		Oscillatory flow		
	C_D	*Re [x10^4]*	C_D	C_M	*KC [-]*
This study	1.6	2.3–14	2.3	2.1	1.9–8.8
Raman-Nair and Colbourne, 2003	1.5	–	–	–	–
Plew, 2005	0.89	0.4–1.2	–	–	–
Raman-Nair et al., 2008	1.2	–	–	–	–
Stevens et al., 2008	1.5	–	–	–	–
Plew et al., 2009	1.3	1.0–7.0	–	–	–
Gagnon and Bergeron, 2011	1.25	3.5–10	–	–	–
Knysh et al., 2020	1.1–1.7	>4.0	–	–	–
Xu et al., 2020	1.1–1.2	0.39–10	–	–	–

- Drag tests with mussel dropper lines were conducted in a wave flume at varying velocities. Based on the results a drag coefficient of $C_D = 1.6$ is recommended for currents with subcritical flow regimes ($Re < 10^5$) and blue mussels (*Mytilus edulis*). Similarly, the mussel dropper lines were subjected to waves and a drag coefficient of $C_D = 2.3$ and an inertia coefficient of $C_M = 2.1$ are proposed for $KC < 10$. Further tests with other commonly cultivated species, e.g. green-lipped mussels (*perna canaliculus*), are suggested. To obtain species specific hydrodynamic parameters. Additional investigations on the hydrodynamic coefficients for large *Re* and *KC*-numbers are of special interest for the envisaged remote offshore aquaculture sites.
- Simultaneously, tests with three surrogate models were carried out and their drag and inertia coefficients under steady and oscillatory flow were quantified. The aim was to obtain a simplified model, which can be used in both physical and numerical experiments without the need for keeping mussels alive or using geometrically divergent forms. The performance of the surrogates deviated from the live mussels under steady current while the performance under oscillatory flow showed a good fit. Surrogate 1, based on the average shell of the originally tested blue mussels, was chosen for further testing as it showed the best fit. Likewise, to the live mussels, investigations of the surrogates with increasing *Re*- and *KC*-numbers are planned for future research.
- This study shows that the choice of the characteristic diameter has a large influence on the hydrodynamic coefficients and the findings suggest a larger characteristic diameter then former studies.
- A comparison to published studies reveals that experimental research regarding the hydrodynamic coefficients of mussel dropper lines is scarce, since most studies focus on drag in steady flow. This study provides estimated inertia coefficients of mussel dropper lines and surrogates based on wave tests.

Future testing of the proposed SM1 should include investigations regarding the scaling potential of the surrogate body to enable further physical investigations of whole shellfish longline systems with increased accuracy as well as larger scale experiments to deepen the understanding regarding larger ranges of *Re*and *KC*. The specific influence of the soft growth and surface roughness on the hydrodynamic parameters of mussel dropper lines was not scope of this study, but is subject to ongoing and future studies. Applying the obtained knowledge to future research, this study provides a basis for the design and evaluation of novel offshore bivalve aquaculture. The insights gathered in this study facilitate the testing procedure for aquaculture systems and provide robust estimates for numerical approaches. This information can be used in the development of novel marine aquaculture systems in the light of the increasing demand for marine protein.

CRediT authorship contribution statement

Jannis Landmann: Conceptualization, Methodology, Writing – original draft, Writing – review & editing. **Lukas Fröhling:** Writing – review & editing. **Rebekka Gieschen:** Writing – review & editing. **Bela H. Buck:** Writing – review & editing. **Kevin Heasman:** Writing – review & editing. **Nicholas Scott:** Writing – review & editing. **Malcolm Smeaton:** Writing – review & editing. **Nils Goseberg:** Conceptualization, Funding acquisition, Writing – review & editing, Supervision. **Arndt Hildebrandt:** Conceptualization, Funding acquisition, Writing – review & editing, Supervision.

Declaration of competing interest

The authors declare that they have no known competing financial interests or personal relationships that could have appeared to influence the work reported in this paper.

Acknowledgments

This Research has been supported with funding from the New Zealand Ministry of Business, Innovation and Employment through Cawthron Institute project CAWX1607. This research has also received support from start-up funds provided by Technische Universität Braunschweig, Germany, to Prof. Nils Goseberg.

References

Abbott, E.J., Firestone, F.A., 1933. Specifying surface quality- A method based on accurate measurement and comparison. Mech. Eng. 55, 569–577.
Achenbach, E., 1971. Influence of surface roughness on the cross-flow around a circular cylinder. J. Fluid Mech. 46, 321. https://doi.org/10.1017/S0022112071000569.
Allen, D.W., Henning, D.L., 2001. Surface roughness effects on vortex-induced vibration of cylindrical structures at critical and supercritical Reynolds numbers. In: 13302, O. (Ed.), Proc. Offshore Technol. Confeuence. https://doi.org/10.4043/13302-ms. Houston, TX.
Atalah, J., Fletcher, L.M., Hopkins, G.A., Heasman, K., Woods, C.M.C., Forrest, B.M., 2016. Preliminary assessment of biofouling on offshore mussel farms. J. World Aquacult. Soc. 47, 376–386. https://doi.org/10.1111/jwas.12279.
Bagheri, G., Bonadonna, C., 2016. On the drag of freely falling non-spherical particles. Powder Technol. 301, 526–544. https://doi.org/10.1016/j.powtec.2016.06.015.
Bonakdar, L., Oumeraci, H., Etemad-Shahidi, A., 2015. Wave load formulae for prediction of wave-induced forces on a slender pile within pile groups. Coast. Eng. 102, 49–68. https://doi.org/10.1016/j.coastaleng.2015.05.003.
Brenner, M., Buck, B.H., 2010. Attachment properties of blue mussel (Mytilus edulis L.) byssus threads on culture-based artificial collector substrates. Aquacult. Eng. 42, 128–139. https://doi.org/10.1016/j.aquaeng.2010.02.001.
Buck, B.H., 2007. Experimental trials on the feasibility of offshore seed production of the mussel Mytilus edulis in the German Bight: installation, technical requirements and environmental conditions. Helgol. Mar. Res. 61, 87–101. https://doi.org/10.1007/s10152-006-0056-1.
Buck, B.H., Langan, R., 2017. Aquaculture Perspective of Multi-Use Sites in the Open Ocean - The Untapped Potential for Marine Resources in the Anthropocene. SpringerOpen. https://doi.org/10.1007/978-3-319-51159-7.
Chakrabarti, A., Chen, Q., Smith, H.D., Liu, D., 2016. Large eddy simulation of unidirectional and wave flows through vegetation. J. Eng. Mech. 142, 1–18. https://doi.org/10.1061/(ASCE)EM.1943-7889.0001087.
Cheney, D., Langan, R., Heasman, K., Friedman, B., Davis, J., 2010. Shellfish culture in the open ocean: lessons learned for offshore expansion. Mar. Technol. Soc. J. 44, 55–67.
Dean, R.G., Dalrymple, R.A., 1991. Water Wave Mechanics for Engineers and Scientists. WORLD SCIENTIFIC. https://doi.org/10.1142/1232.
Denny, M., 1995. Predicting physical disturbance: mechanistic approaches to the study of survivorship on wave-swept shores. Ecol. Monogr. 65, 371–418. https://doi.org/10.2307/2963496.
Díaz, C., Figueroa, Y., Sobenes, C., 2011. Effect of different longline farming designs over the growth of Mytilus chilensis (Hupé, 1854) at Llico Bay, VIII Región de Bio-Bio, Chile. Aquacult. Eng. 45, 137–145. https://doi.org/10.1016/j.aquaeng.2011.09.002.
DNV, 2010a. DNV-RP-F205: Global Performance Analysis of Deepwater Floating Structures. https://rules.dnvgl.com/docs/pdf/DNV/codes/docs/2010-10/RP-F205.pdf, 28.
DNV, 2010b. DNV-RP-C205 Dnv. Environmental conditions and environmental loads. https://doi.org/10.1109/INTLEC.1993.388591, 124.
Drapeau, A., Comeau, L.A., Landry, T., Stryhn, H., Davidson, J., 2006. Association between longline design and mussel productivity in Prince Edward Island. Can. Aquacult. 261, 879–889. https://doi.org/10.1016/j.aquaculture.2006.07.045.
Fao, 2020. The State of World Fisheries and Aquaculture 2020. FAO, Rome. https://doi.org/10.4060/ca9229en.
Gagnon, M., 2019. Self-organization and mechanical properties of mussel culture suspensions: a critical review. Aquacult. Eng. 87, 102024. https://doi.org/10.1016/j.aquaeng.2019.102024.
Gagnon, M., Bergeron, P., 2011. Propriétés mécaniques des composantes des filières maricoles du Québec. Québec, Canada.
Gagnon, M., Bergeron, P., 2017. Observations of the loading and motion of a submerged mussel longline at an open ocean site. Aquacult. Eng. 78, 114–129. https://doi.org/10.1016/j.aquaeng.2017.05.004.
Garen, P., Robert, S., Bougrier, S., 2004. Comparison of growth of mussel, Mytilus edulis, on longline, pole and bottom culture sites in the Pertuis Breton. France, Aquaculture 232, 511–524. https://doi.org/10.1016/S0044-8486(03)00535-0.
Gentry, R.R., Froehlich, H.E., Grimm, D., Kareiva, P., Parke, M., Rust, M., Gaines, S.D., Halpern, B.S., 2017. Mapping the global potential for marine aquaculture. Nat. Ecol. Evol. 1, 1317–1324. https://doi.org/10.1038/s41559-017-0257-9.
Heasman, K., Pitcher, G.C., McQuaid, C.D., Hecht, T., 1998. Shellfish mariculture in the benguela system: raft culture of Mytilus Galloprovincialis and the effect of rope spacing on food extraction, growth rate, production, and condition of mussels. J. Shellfish Res. 17, 33–39.
Heasman, K., Scott, N., Smeaton, M., Goseberg, N., Hildebrandt, A., Vitasovich, P., Elliot, A., Mandeno, M., Buck, B.H., 2021. New system design for the cultivation of extractive species at exposed sites - Part 1: System design, deployment and first

response to high-energy environments. Applied Ocean Research 110. https://doi.org/10.1016/j.apor.2021.102603.
Henchion, M., Hayes, M., Mullen, A., Fenelon, M., Tiwari, B., 2017. Future protein supply and demand: strategies and factors influencing a sustainable equilibrium. Foods 6, 53. https://doi.org/10.3390/foods6070053.
Hildebrandt, A., Sparboom, U., Oumeraci, H., 2009. Wave forces ON groups OF slender cylinders IN comparison to an isolated cylinder due to NON-breaking waves. In: Coast. Eng. 2008. World Scientific Publishing Company, pp. 3770–3781. https://doi.org/10.1142/9789814277426_0312.
Hildebrandt, A., Landmann, J., Ongsiek, T., Goseberg, N., 2018. Drag coefficients of vertically-mounted full-scale blue mussel dropper lines. In: Proc. Int. Conf. Offshore Mech. Arct. Eng. - OMAE. https://doi.org/10.1115/OMAE201878534.
Hosomi, R., Yoshida, M., Fukunaga, K., 2012. Seafood consumption and components for health. Global J. Health Sci. 4, 72–86. https://doi.org/10.5539/gjhs.v4n3p72.
Joschko, T.J., Buck, B.H., Gutow, L., Schröder, A., 2008. Colonization of an artificial hard substrate by Mytilus edulis in the German Bight. Mar. Biol. Res. 4, 350–360. https://doi.org/10.1080/17451000801947043.
Keulegan, G.H., Carpenter, L.H., 1934. Forces on cylinders and plates in an oscillating fluid. J. Res. Natl. Bur. Stand. 60, 423–440, 1958.
Knysh, A., Tsukrov, I., Chambers, M., Swift, M.R., Sullivan, C., Drach, A., 2020. Numerical modeling of submerged mussel longlines with protective sleeves. Aquacult. Eng. 88, 102027. https://doi.org/10.1016/j.aquaeng.2019.102027.
Konstantinou, Z.I., Kombiadou, K., 2020. Rethinking suspended mussel-farming modelling : combining hydrodynamic and bio-economic models to support integrated aquaculture management. Aquaculture 523, 735179. https://doi.org/10.1016/j.aquaculture.2020.735179.
Landmann, J., Fröhling, L., Gieschen, R., Buck, B.H., Heasman, K., Scott, N., Smeaton, M., Goseberg, N., Hildebrandt, A., 2021. New system design for the cultivation of extractive species at exposed sites - Part 2: Experimental modelling in waves and current. Applied Ocean Research 113. https://doi.org/10.1016/j.apor.2021.102749.
Landmann, J., Ongsiek, T., Goseberg, N., Heasman, K., Buck, B.H.B.H., Paffenholz, J.-A. J.-A., Hildebrandt, A., 2019. Physical modelling of blue mussel dropper lines for the development of surrogates and hydrodynamic coefficients. J. Mar. Sci. Eng. 7, 65. https://doi.org/10.3390/jmse7030065.
Le Méhauté, B., 1976. An Introduction to Hydrodynamics & Water Waves. Springer Science + Business Media, LLC. https://doi.org/10.1007/978-3-642-85567-2.
Lin, J., Li, C., Zhang, S., 2016. Hydrodynamic effect of a large offshore mussel suspended aquaculture farm. Aquaculture 451, 147–155. https://doi.org/10.1016/j.aquaculture.2015.08.039.
Liu, Z., Huguenard, K., 2020. Hydrodynamic response of a floating aquaculture farm in a low inflow estuary. J. Geophys. Res. Ocean. 125 https://doi.org/10.1029/2019JC015625.
Loth, E., 2008. Drag of non-spherical solid particles of regular and irregular shape. Powder Technol. 182, 342–353. https://doi.org/10.1016/j.powtec.2007.06.001.
Morison, J.R., O'Brien, M.P., Johnson, J.W., Schaaf, S.A., O'Brien, M.P., Johnson, J.W., Schaaf, S.A., 1950. The forces exerted by surface waves on piles. Pet. Trans. AIME. 189, 149–157.
Nath, J.H., 1987. On wave force coefficient variability. J. Offshore Mech. Arctic Eng. 109, 295–306. https://doi.org/10.1115/1.3257023.
Negro, V., López-Gutiérrez, J.-S., Esteban, M.D., Matutano, C., 2014. Uncertainties in the design of support structures and foundations for offshore wind turbines. Renew. Energy 63, 125–132. https://doi.org/10.1016/j.renene.2013.08.041.
Obasaju, E.D., Bearman, P.W., Graham, J.M.R., 1988. A study of forces, circulation and vortex patterns around a circular cylinder in oscillating flow. J. Fluid Mech. 196, 467–494.
O'Donncha, F., Hartnett, M., Nash, S., 2013. Physical and numerical investigation of the hydrodynamic implications of aquaculture farms. Aquacult. Eng. 52, 14–26. https://doi.org/10.1016/j.aquaeng.2012.07.006.
Plew, D.R., 2005. The Hydrodynamic Effects of Long-Line Mussel Farms.
Plew, D.R., Stevens, C.L., Spigel, R.H., Hartstein, N.D., 2005. Hydrodynamic implications of large offshore mussel farms. IEEE J. Ocean. Eng. 30, 95–108. https://doi.org/10.1109/JOE.2004.841387.
Plew, D.R., Enright, M.P., Nokes, R.I., Dumas, J.K., 2009. Effect of mussel bio-pumping on the drag on and flow around a mussel crop rope. Aquacult. Eng. 40, 55–61. https://doi.org/10.1016/j.aquaeng.2008.12.003.
Raman-Nair, W., Colbourne, B., 2003. Dynamics of a mussel longline system. Aquacult. Eng. 27, 191–212. https://doi.org/10.1016/S0144-8609(02)00083-3.
Raman-Nair, W., Colbourne, B., Gagnon, M., Bergeron, P., 2008. Numerical model of a mussel longline system: coupled dynamics. Ocean. Eng. 35, 1372–1380. https://doi.org/10.1016/j.oceaneng.2008.05.008.
Reid, G.K., Lefebvre, S., Filgueira, R., Robinson, S.M.C., Broch, O.J., Dumas, A., Chopin, T.B.R., 2020. Performance measures and models for open-water integrated multi-trophic aquaculture. Rev. Aquacult. 12, 47–75. https://doi.org/10.1111/raq.12304.
Reynolds, O., 1883. An experimental investigation of the circumstances which determine whether the motion of water shall be direct or sinuous, and of the law of resistance in parallel channels. Phil. Trans. Roy. Soc. Lond. 174, 935–982. https://doi.org/10.1098/rstl.1883.0029.
Röös, E., Bajzelj, B., Smith, P., Patel, M., Little, D., Garnett, T., 2017. Protein futures for Western Europe : potential land use and climate impacts in 2050. Reg. Environ. Change 17, 367–377. https://doi.org/10.1007/s10113-016-1013-4.
Rosland, R., Bacher, C., Strand, Ø., Aure, J., Strohmeier, T., 2011. Modelling growth variability in longline mussel farms as a function of stocking density and farm design. J. Sea Res. 66, 318–330. https://doi.org/10.1016/j.seares.2011.04.009.
Sarpkaya, T., 1976. Vortex shedding and resistance in harmonic flow about smooth and rough circular cylinders at high Reynolds numbers. Monterey, California.
Sarpkaya, T., 1987. Oscillating flow about smooth and rough cylinders. Proc. ASME Sixth Int. Offshore Mech. Arct. Eng. Symp. II, J.S. C 307–313.
Sarpkaya, T., 1990. On the effect of roughness on cylinders. J. Offshore Mech. Arctic Eng. 112, 334. https://doi.org/10.1115/1.2919875.
Sarpkaya, T., Bakmis, C., Storm, M.A., 1984. Hydrodynamic forces from combined wave and current flow on smooth and rough circular cylinders at high Reynolds numbers. Offshore Technol. Conf. 455–462. https://doi.org/10.4043/4830-MS.
Shi, J., Wei, H., Zhao, L., Yuan, Y., Fang, J., Zhang, J., 2011. A physical-biological coupled aquaculture model for a suspended aquaculture area of China. Aquaculture 318, 412–424. https://doi.org/10.1016/j.aquaculture.2011.05.048.
Stevens, C.L., Plew, D.R., Smith, M.J., Fredriksson, D.W., 2007. Hydrodynamic forcing of long-line mussel farms: Observations. J. Waterw. Port, Coast. Ocean Eng. 133, 192–199. https://doi.org/10.1061/(ASCE)0733-950X, 2007)133:3(192.
Stevens, C.L., Plew, D.R., Hartstein, N., Fredriksson, D., 2008. The physics of open-water shellfish aquaculture. Aquacult. Eng. 38, 145–160. https://doi.org/10.1016/j.aquaeng.2008.01.006.
Sumer, B.M., Fredsoe, J., 2006. Hydrodynamics Around Cylindrical Structures. World Scientific Publishing Co. Pte. Ltd.
Telesca, L., Michalek, K., Sanders, T., Peck, L.S., Thyrring, J., Harper, E.M., 2018. Blue mussel shell shape plasticity and natural environments : a quantitative approach. Sci. Rep. 1–15. https://doi.org/10.1038/s41598-018-20122-9.
Wolfram, J., Naghipour, M., 1999. On the estimation of Morison force coefficients and their predictive accuracy for very rough circular cylinders. Appl. Ocean Res. 21, 311–328. https://doi.org/10.1016/S0141-1187(99)00018-8.
Wolfram, J., Theophanatos, A., 1985. The effects of marine fouling on the fluid loading of cylinders: some experimental results. In: Proc. Annu. Offshore Technol. Conf., pp. 517–526. https://doi.org/10.4043/4954-ms.
Wolfram, J., Theophanatos, A., 1990. Marine roughness and fluid loading, environ. Forces offshore struct. Their predict. Proc. Int. Conf. 22.
Xu, T., Dong, G., 2018. Numerical simulation of the hydrodynamic behaviour of mussel farm in currents. Ships Offshore Struct. 1–12. https://doi.org/10.1080/17445302.2018.1465380, 0.
Xu, Z., Qin, H., Li, P., Liu, R., 2020. Computational fluid dynamics approaches to drag and wake of a long-line mussel dropper under tidal current. Sci. Prog. 103, 1–25. https://doi.org/10.1177/0036850419901235.
Zhao, Y.-P., Yang, H., Bi, C., Chen, Q.-P., Dong, G.-H., Cui, Y., 2019. Hydrodynamic responses of longline aquaculture facility with lantern nets in waves. Aquacult. Eng. 86, 101996. https://doi.org/10.1016/j.aquaeng.2019.101996.
Zhu, L., Huguenard, K., Zou, Q., Fredriksson, D.W., Xie, D., 2020. Aquaculture farms as nature-based coastal protection : random wave attenuation by suspended and submerged canopies. Coast. Eng. 160, 103737. https://doi.org/10.1016/j.coastaleng.2020.103737.